Title

Tyrosine kinase inhibitors affect sweet taste and dysregulate fate selection of specific taste cell subtypes via KIT inhibition.

Authors

Christina M. Piarowski[1,2], Jennifer K. Scott[1,2], Courtney E. Wilson[1,2], Heber I. Lara[3], Ernesto Salcedo[1], Andrew S. Han[1,6], Elaine T. Lam[4], Peter J. Dempsey[5], Jakob von Moltke[3], Linda A. Barlow[1,2] *

* Corresponding author: Linda.barlow@cuanschutz.edu

Affiliations

[1]Department of Cell and Developmental Biology, University of Colorado Anschutz Medical Campus, Aurora Colorado.
[2] Rocky Mountain Taste and Smell Center, University of Colorado Anschutz Medical Campus, Aurora Colorado.
[3] Department of Immunology, University of Washington, Seattle Washington.
[4] Department of Medical Oncology, University of Colorado Anschutz Medical Campus, Aurora Colorado.
[5]Department of Pediatrics, Section of Developmental Biology, University of Colorado Anschutz Medical Campus, Aurora Colorado.
[6]Developing Scholars Internship Program, Graduate Program in Cell Biology, Stem Cells and Development, University of Colorado Anschutz Medical Campus.

Abstract

Taste dysfunction, or dysgeusia, is a common side effect of many cancer drugs. Dysgeusia is often reported by patients treated with anti-angiogenic tyrosine kinase inhibitors (TKIs), which inhibit receptor tyrosine kinases (RTKs). However, the mechanisms by which TKIs cause dysgeusia are not understood, as the role of RTKs in adult taste homeostasis is unknown. Here, we find that treating adult mice with the TKI cabozantinib shifts the fate of differentiating functional taste cell subtypes within taste buds. Through behavioral assays, we find this cell fate shift leads to blunted responses to sweet tastant in cabozantinib-treated mice. Finally, we show that inducible knockout of the RTK KIT, which is inhibited by cabozantinib, largely phenocopies drug treatment. Our results establish KIT as a regulator of taste cell homeostasis and suggest that KIT inhibition may underlie TKI-induced dysgeusia in patients.

Teaser

KIT signaling blockade by tyrosine kinase inhibitors alters the fate of functional taste bud cell subtypes.

Introduction

The sense of taste, or gustation, plays a central role in how animals experience the world. Taste conveys important nutritional information through five modalities: sweet, bitter, umami, sour, and salty [1]. Taste dysfunction (dysgeusia) is a common side effect of many cancer therapies [2] that can lead to significantly reduced quality of life, including weight loss and depression, as well as worsened long-term outcomes in cancer patients [3, 4]. Improving both

quality of life and treatment outcomes therefore necessitates interventions that mitigate or prevent this side effect. However, the field lacks important mechanistic understanding of how most cancer drugs affect the taste system [2].

One class of targeted cancer therapies that commonly cause dysgeusia are anti-angiogenic tyrosine kinase inhibitors (TKIs). These TKIs reduce tumor vascularization by targeting vascular endothelial growth factor receptors (VEGFRs) and platelet-derived growth factor receptor beta (PDGFRβ), both of which are receptor tyrosine kinases (RTKs) [5-7]. A subset of anti-angiogenic TKIs, including cabozantinib, axitinib and sunitinib, are approved as first- and second-line therapies for metastatic renal cell carcinoma (mRCC) and cause dysgeusia in 10-50% of mRCC patients [5, 8-10]. However, the intended targets, VEGFRs and PDGFRβ, are rarely found in epithelial cells, as they are primarily expressed in endothelial and stromal cells [11, 12]. Further, transcriptome analyses have not identified expression of VEGFRs or PDGFRβ mRNAs in murine taste epithelium [13-18]. Cabozantinib, axitinib, and sunitinib, as well as TKIs more generally, inhibit many off-target RTKs including RET, MET, KIT, PDGFRα, epidermal growth factor receptors (EGFRs), fibroblast growth factor receptors (FGFRs) and insulin-like growth factor receptors (IGFRs) [19-21]. Many of these off-target RTKs are expressed in taste epithelium [14, 16, 22-26], raising the possibility that inhibition of one or more off-target RTKs underlies TKI-induced dysgeusia

Taste is mediated by taste buds, which are collections of 50-100 specialized epithelial taste bud cells (TBCs) that comprise three morphological types [27, 28]. Type I cells are glial-like support cells, type II cells detect sweet, bitter, or umami tastants, while type III cells detect sour and some salty tastants [1, 29-31]. Taste buds also house specialized salt-sensitive cells similar to type II cells in morphology and expression of many but not all type II cell markers [32-34]. TBCs are short-lived and turn over with lifespans ranging from 10 to 40 days [35-39]. All TBCs as well as non-taste cells that surround taste buds are generated by proliferating progenitors outside of buds [40, 41]. Despite continual turnover, the proportions of TBC types are relatively stable throughout life [40]. Thus, the renewal process, spanning progenitor proliferation to TBC fate specification, differentiation, and survival, must be tightly regulated to ensure reliable taste function over time. As TKIs used to treat mRCC are frequently associated with taste dysfunction [5, 10], characterizing how these drugs impact taste homeostasis may provide cell and molecular insight into how they cause dysgeusia.

In rodents, taste buds on the tongue are housed in three taste fields: fungiform papillae (FFP) in the anterior tongue typically contain one taste bud each, while in the posterior tongue, a single circumvallate papilla (CVP) at the posterior midline and bilateral foliate papillae comprise invaginated epithelial trenches that house hundreds of taste buds [42]. Importantly, taste buds in all papillae detect sweet, sour, bitter, etc., although bitter sensitivity is greater in the posterior tongue while sweet sensitivity is greater in the anterior tongue [43, 44]. Specialized salt-sensing cells are found only in FFP taste buds [32]. How TKIs impact taste buds, and whether their impact differs based on taste field, is not known.

Here, we investigate the effects of anti-angiogenic TKIs on taste homeostasis using both lingual organoids and mouse models. We show that cabozantinib affects renewal of type II TBC subtypes by dysregulating their differentiation, leading to changes in cell type composition. We also find that TKI-induced alteration of type II subtype fate differs between FFP and CVP taste buds. Cellular changes in CVP but not FFP taste buds correspond with changes to behavioral taste preferences, linking dysregulation of type II TBC fate selection with dysgeusia. Finally, we find that inhibition of the off-target RTK KIT likely regulates renewal of TBC subtypes, as

inducible *Kit* knockout largely phenocopies TKI treatment. This work provides insight into the regulation of type II TBC subtype fate selection and establishes KIT signaling in this process.

Results

TKIs selectively affect sweet type II TBCs in lingual organoids

We first used lingual organoids to screen the effects of TKIs on taste bud homeostasis. These are generated from isolated taste progenitor cells that proliferate and differentiate into organoids containing non-taste cells and all TBC types [45]. Organoids were generated from GFP^+ taste progenitors from the CVP epithelium of adult $Lgr5^{CreER\text{-}eGFP}$ mice [45]. We first assessed if three TKIs used in treatment of mRCC patients, cabozantinib, axitinib, and sunitinib [8, 9], hindered cell proliferation and/or organoid survival during the growth phase of culture (days 2-6) (**Figure S1A**).

To quantify cell proliferation, 5-ethynyl-2'-deoxyuridine (EdU) was added to cultures for 30 minutes prior to harvest (**Figure S1A**). TKI treatment did not alter EdU incorporation by organoids (**Figure S1B-C**). We further assessed organoid growth by quantifying organoid size at day 6. Organoids treated with paclitaxel, which blocks cell proliferation [46] and was used as a positive control, were significantly smaller than vehicle controls, whereas TKI treatment had little to no impact on organoid growth (**Figure S2A**). While organoid size was significantly decreased by 100nM axitinib, this difference was small compared to treatment with paclitaxel (**Figure S2A**). Results with a Cell-Titer Glo® 3D cell viability assay, which measures ATP luminescence as a proxy for cell survival, were congruent with organoid size; paclitaxel decreased luminescence compared to control organoids, whereas TKI treatment, including 100nM axitinib, had no impact (**Figure S2B**). Lastly, we quantified organoid survival at day 6 and found 40-60% of isolated *Lgr5*-GFP^+ progenitors formed organoids that survived regardless of condition (**Figure S2C-D**). In sum, our data indicate that cabozantinib, axitinib, and sunitinib do not affect taste progenitor proliferation or survival *in vitro*.

To test if TKIs affect TBC differentiation, we treated organoids during the differentiation phase of culture (days 6-12) (**Figure 1A**). On day 12, organoids were harvested for immunostaining for markers of type I ($NTPDase2^+$)[47], type II ($PLC\beta2^+$)[48], and type III ($CAR4^+$)[49] TBCs. We found that prevalence of TBC types did not differ in TKI-treated versus control organoids (**Figures 1B-C**, **S3A-D**). Type II TBCs comprise functional subsets, and those in the CVP that detect bitter and umami express the G-protein GUSTDUCIN (GUST) [50]. $GUST^+$ TBC prevalence likewise was unaffected by TKI treatment (**Figure 1D-E**). Thus, TKIs did not impact the differentiation of type I, II, or III TBCs, nor bitter/umami type II TBCs, *in vitro*.

To determine if TKIs affected other taste epithelial cell populations, we expanded our panel of markers using RT-qPCR. Expression of *Kcnq1*, expressed by all TBCs [51], and *Krt13*, a marker of non-taste epithelium [52], were unchanged by drug treatment, suggesting that production of taste versus non-taste lineages was unaffected by TKIs (**Figure S3E-F**). Consistent with immunostaining, markers of type I (*Kcnj1*)[53], type II (*Plcβ2*), and type III (*Pkd2l1*)[54] TBCs, as well as bitter/umami TBCs (*Gnat3* - encodes GUST) were unaffected by TKIs (**Figures 1F-G**, **S3G-H**). Surprisingly, however, markers of the sweet subset of type II TBCs were specifically reduced. Expression of the G-protein coupled receptor *Tas1r2,* which heterodimerizes with TAS1R3 to mediate sweet tastant transduction [55], was decreased significantly by all three TKIs (**Figure 1H).** *Pcdh20*, another sweet cell marker [56], was

decreased significantly by cabozantinib and expression trended downward with sunitinib (p=0.07) (**Figure 1I).** These data suggested that TKIs selectively affect sweet type II TBCs, but not other cell types, in lingual organoids.

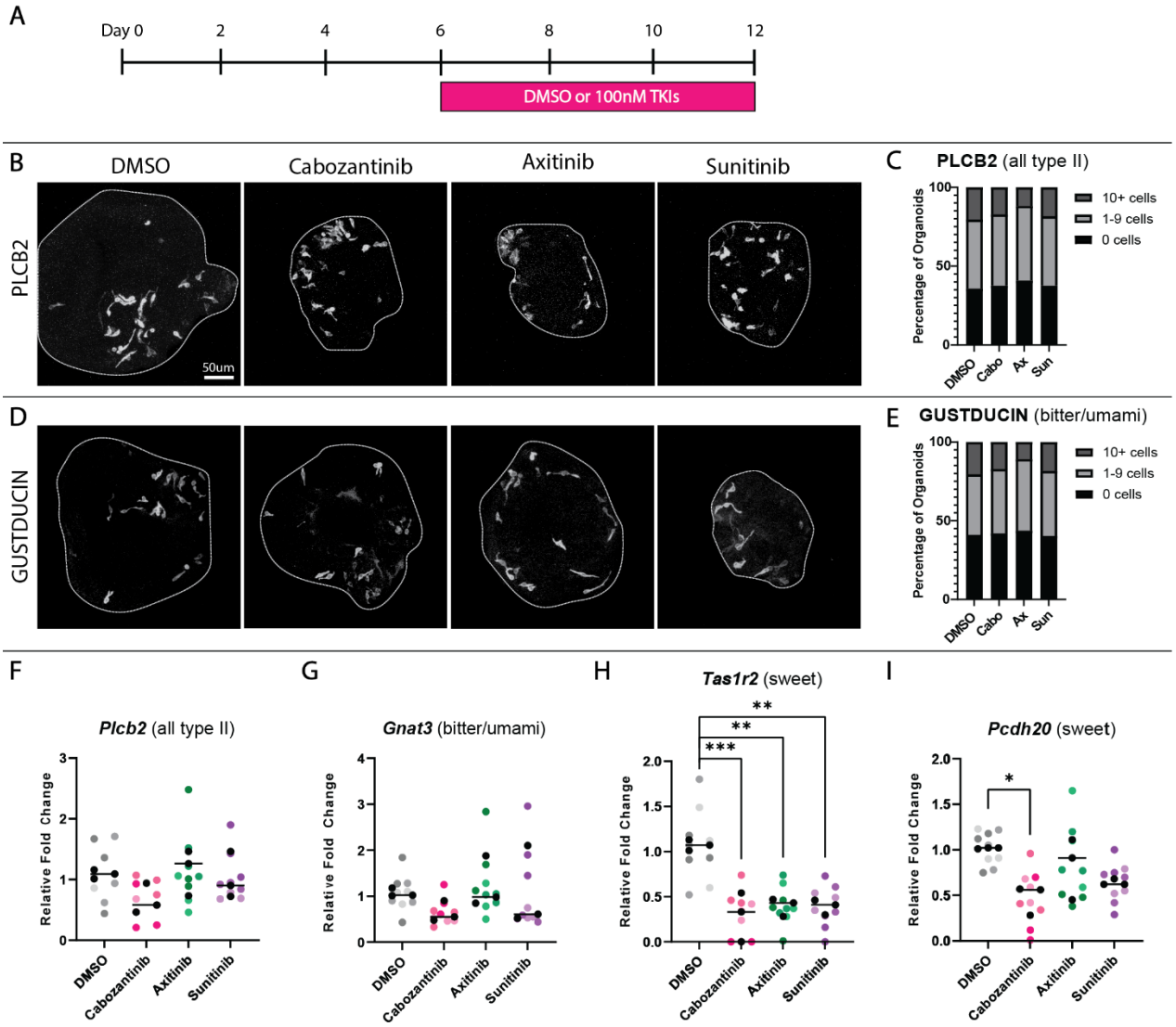

Figure 1: TKIs selectively affect markers of sweet type II TBCs in lingual organoids. (**A**) Experimental design to test cabozantinib (Cabo), axitinib (Ax), and sunitinib (Sun) on TBC differentiation in organoids. (**B-E**) Compressed confocal z-stacks of control and TKI-treated organoids immunostained for markers of type II TBCs, PLCβ2 (**B**) and bitter/umami type II TBCs, GUSTDUCIN (**D**). Percentages of organoids containing 0, 1-9, or ≥ 10 cells immunopositive for PLCβ2 (**C**) or GUSTDUCIN (**E**) reveal no difference between drug treatment and controls. Total organoids from 3 independent experiments: DMSO - 112; cabo - 93; ax - 110; sun - 109. (**F-I**) Relative fold change in type II TBC marker expression via RT-qPCR. Each colored dot represents an individual sample with organoids pooled from 3 culture wells (~240 organoids per sample). Within a condition, different shades represent 3 biological replicates, and black dots are averages of each replicate. Ordinary one-way ANOVA with Dunnett's multiple comparisons test (panels F-G) or Holm-Sidak's multiple comparisons test

(panel I) were used to compare average values (black line) for each marker across conditions (* $p \leq 0.05$, ** $p \leq 0.01$, *** $p \leq 0.001$).

Cabozantinib changes the cellular composition of taste buds *in vivo*

Since sweet TBC marker expression was reduced by TKIs *in vitro*, we asked if TKI treatment specifically affected sweet type II TBCs in adult mice. Cabozantinib was used for *in vivo* experiments because of its long half-life (~120 hours)[57], and because it significantly reduced expression of both sweet TBC markers in organoids (**Figure 1**). Wild-type mice were dosed with vehicle or cabozantinib for 2 weeks (daily) or 4 weeks (5 days/week) (**Figure 2A-B**). Since taste buds in both the anterior and posterior tongue mediate taste, both FFP and CVP were harvested. Cabozantinib was well-tolerated by the mice, whose weights were stable over 4 weeks (**Figure S4A**). Taste buds were also grossly unaffected by drug treatment; mice given cabozantinib had comparable numbers of CVP and FFP taste buds compared to controls, and taste bud size did not differ with treatment (**Figure S4B-I**). These data suggest that cabozantinib does not affect progenitor cell output or overall renewal of taste buds, consistent with data from organoids (**Figures S1-S2**).

To investigate cellular changes within taste buds, we first assessed the prevalence of type II (PLCβ2$^+$) and type III (SNAP25$^+$) TBCs [58] in the CVPs of drug-treated vs control mice. As expected from results in organoids, cabozantinib did not alter the number of type II or III cells (**Figure 2C-H**). We next assessed the prevalence of sweet vs bitter/umami type II TBCs. Consistent with reduced *Tas1r2* expression in organoids, drug treatment significantly diminished the number of *Tas1r2*$^+$ sweet TBCs (**Figure 2I-K**). In contrast to organoids, however, where GUST$^+$ type II TBCs were unaffected, cabozantinib increased GUST$^+$ type II cells in mice (**Figure 2L-N**). Thus, while the total number of type II cells was unaffected, TKI treatment caused a shift in type II TBC subtype composition; *Tas1r2*$^+$ sweet cells were reduced with a concomitant increase in GUST$^+$ bitter/umami cells. Importantly, this phenotype was progressively robust with longer drug treatment (**Figure 2**), suggesting that the shift in type II subtypes depends on gradual turnover of TBCs.

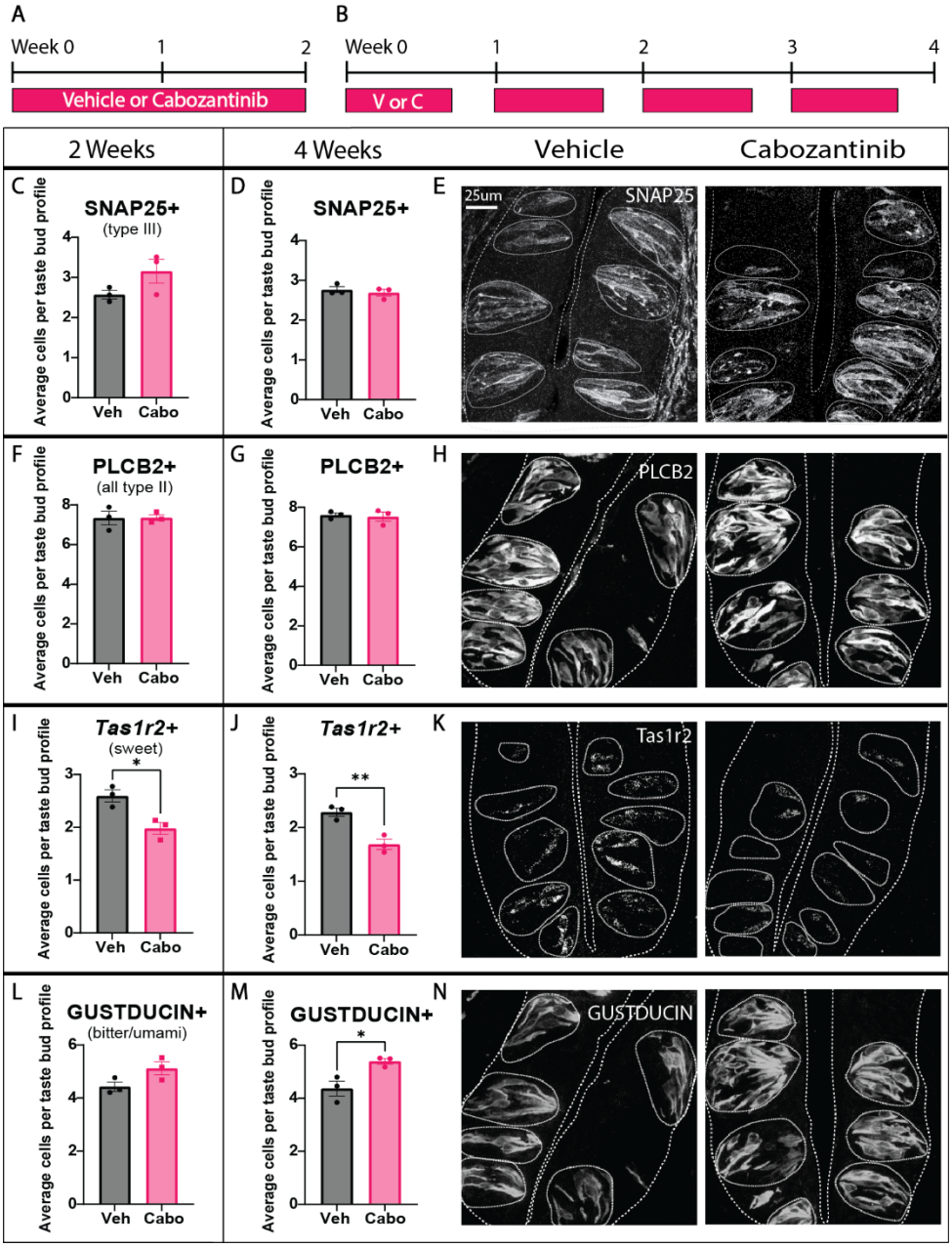

Figure 2: Cabozantinib changes the composition of type II TBC subtypes in CVP taste buds. Mice were treated daily for 2 weeks (**A**) or 5 days per week for 4 weeks with drug or vehicle (**B**). (**C-N**) Quantification of the average number of stained cells per taste bud profile with corresponding representative images for SNAP25 immunofluorscence (IF) (**C-E**), PLCβ2 IF (**F-H**), *Tas1r2* HCR *in situ* hybridization (**I-K**) and GUSTDUCIN IF (**L-N**). Representative images are compressed confocal z-stacks. Coarse dashed lines delineate basement membrane and apical epithelial surface, fine dashed lines encircle individual taste buds. Scale bar in E applies to H, K, and N. In all histograms, each dot represents the average taste cell tally from each mouse (N=3 per condition, ~80 taste buds/mouse). Unpaired t-test. Mean +/- SEM (* $p \leq 0.05$, ** $p \leq 0.01$).

In vivo TKI treatment revealed an increase in GUST$^+$ bitter/umami cells not seen in organoids. Interestingly, we find that GUST$^+$ type II cells are over-represented in CVP-derived organoids compared to CVP taste buds *in vivo* (80% vs 60%, respectively, of PLCβ2$^+$ type II cells are GUST$^+$) (**Figure S5A-B**). This over-representation of GUST$^+$ TBCs in organoids may have obscured subtle increases in this cell population.

We also assessed TBC composition in FFP taste buds after 4 weeks of cabozantinib. As in the CVP, TKI treatment did not affect the total number of PLCβ2$^+$ type II nor SNAP25$^+$ type III cells (**Figure S6A-D**). In FFP, PLCβ2+ type II cells comprise 3 functional subtypes: sweet-, bitter/umami-, and salt-sensing. Unlike in the CVP, where *Tas1r2* and GUST are expressed by separate PLCβ2+ cell populations (sweet versus bitter/umami, respectively), almost all *Tas1r2*$^+$ sweet cells in FFP co-express GUST, as do most bitter and umami type II cells [50, 59]. In contrast, specialized salt-sensing TBCs express PLCβ2 and have strong developmental, molecular and morphological similarities with type II cells, but lack GUST expression [32, 34]. In FFP, despite these differences, cabozantinib nonetheless impacted type II subtype composition; *Tas1r2*$^+$/GUST$^+$ sweet cells were not diminished by drug treatment, nor were GUST$^+$ bitter/umami cells impacted (**Figure S6I-J**). Instead, cabozantinib led to fewer PLCβ2$^+$/GUST$^-$ salt-sensing cells (**Figure S6E-H**). Thus, TKI treatment specifically affects the composition of PLCβ2$^+$ type II TBC subtypes in both FFP and CVP.

Cabozantinib does not shift cell type composition via cell death or transdifferentiation

As cabozantinib significantly reduced *Tas1r2*$^+$ sweet cells in the CVP, we reasoned this loss could be due to: (1) decreased sweet TBC survival, (2) transdifferentiation of sweet cells into bitter/umami cells, or (3) a shift in fate of newly differentiated type II cells. A previous study revealed that the RTK KIT is expressed by TAS1R3$^+$ TBCs, which encompass sweet and umami type II cell subtypes in CVP [23]. Using hybridization chain reaction (HCR) *in situ* hybridization, we found that *Kit* co-localizes with *Tas1r2* in CVP taste buds (**Figure S7A**). Consistent with co-expression of *Tas1r2* and *Kit* in the CVP, and a decrease in *Tas1r2*$^+$ cells in drug-treated mice (see **Figure 2**), cabozantinib significantly decreased the number of KIT$^+$ TBCs per CVP taste bud profile (**Figure S7B-D**). These results indicate that *Kit* is expressed by *Tas1r2*$^+$ sweet type II cells in CVP taste buds.

To assess the fate of differentiated sweet cells following drug treatment, we induced lineage tracing in *Kit*$^{CreER/+}$;*Rosa26*$^{YFP/YFP}$ mice to label existing sweet cells and then treated animals with vehicle or drug for 2 weeks (**Figure 3A**). If cabozantinib inhibits sweet cell survival, then we expected fewer lineage traced *Kit*-YFP$^+$ cells with drug treatment. However, *Kit*-YFP$^+$ cell number did not differ in vehicle- versus cabozantinib-treated mice, indicating no impact on sweet cell survival (**Figure 3B-C**). We next examined type II subtype identity of *Kit*-YFP$^+$ cells to determine if cabozantinib caused transdifferentiation of differentiated sweet cells, potentially into GUST$^+$ bitter/umami cells. As expected, most *Kit*-YFP$^+$ cells were PLCβ2$^+$ type II cells in controls (**Figure 3D-E**). Of these, ~85% were *Tas1r2*$^+$ sweet cells with very few GUST$^+$ bitter/umami cells (**Figure 3F-I**). Since the *Kit*-YFP lineage included a small percentage of GUST$^+$ cells in controls, this suggests that *Kit* is either expressed in a subset of differentiated bitter/umami cells, or in cells that give rise to both *Tas1r2*$^+$ and GUST$^+$ cells. Importantly, cabozantinib did not change the percentage of *Kit*-YFP$^+$ cells expressing *Tas1r2* or GUST (**Figure 3F-I**), demonstrating that differentiated sweet cells in the CVP maintain their identity and do not transdifferentiate into bitter/umami type II TBCs with drug treatment.

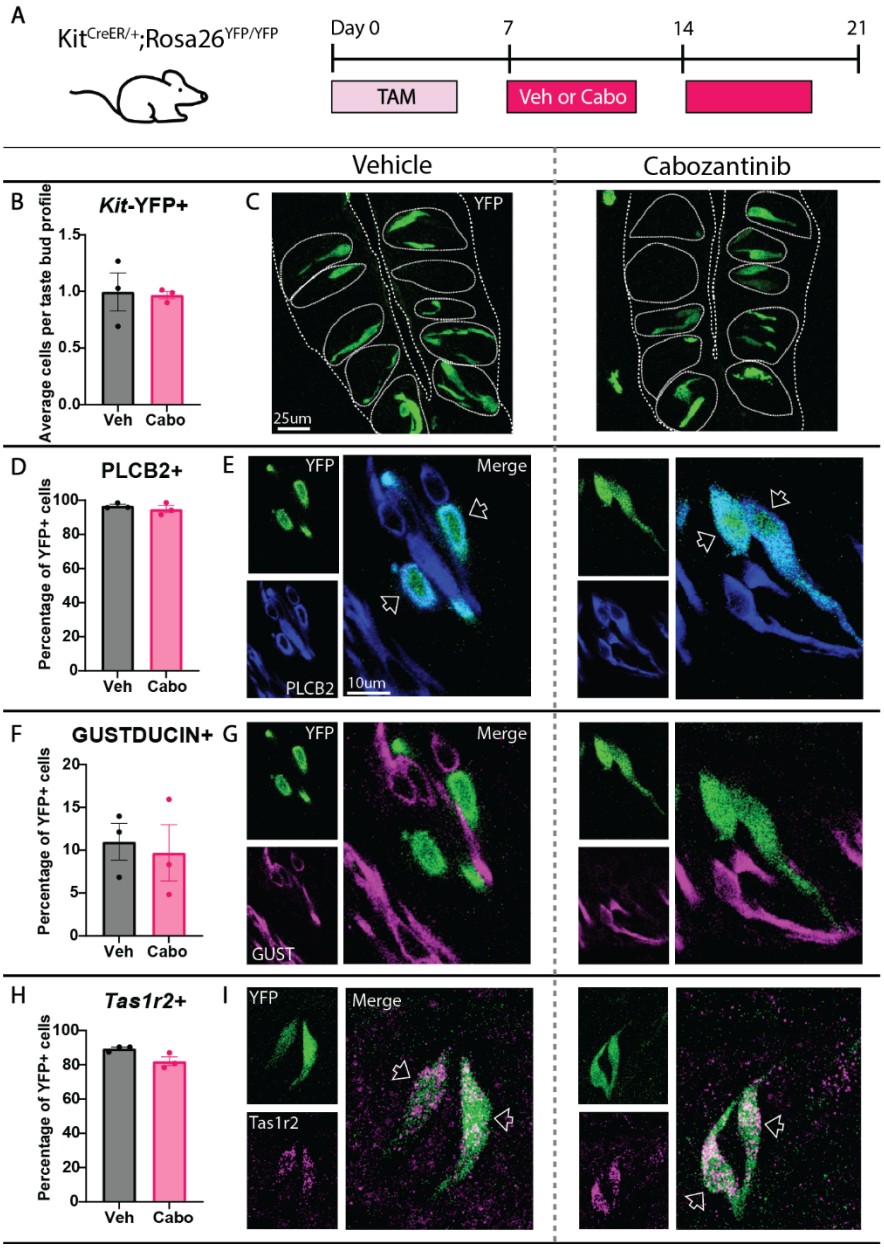

Figure 3: Cabozantinib does not reduce survival or induce transdifferentiation of sweet type II TBCs in CVP taste buds. (**A**) *Kit$^{CreER/+}$;Rosa26$^{YFP/YFP}$* mice were gavaged with tamoxifen daily for 5 days. Following a 3-day chase with daily cage changes, mice were gavaged with vehicle or cabozantinib 5 days per week for 14 days. (**B**) *Kit*-YFP^{+} cells per taste bud profile were unaltered by TKI treatment. (**C**) Compressed confocal z-stacks of *Kit*-YFP+ taste cells in CVP taste buds from vehicle- vs cabozantinib-treated mice. Coarse dashed lines delineate basement membrane and apical epithelial surface, fine dashed lines encircle individual taste buds. (**D-I**) The percentage of *Kit*-YFP^{+} cells (green in all panels) co-expressing PLCβ2 (**D-E, blue in E** optical section), GUSTDUCIN (**F-G, Magenta in G**, optical section), or *Tas1r2* (**H-I, magenta in I**, compressed z-stack), is unchanged by drug treatment. Empty arrowheads in E and I indicate double-labeled cells. In panels D and F, values were calculated across 232 YFP^{+} cells and 247 taste buds in vehicle mice and 224 YFP^{+} cells and 262 taste buds in cabozantinib mic,

and in H across 243 YFP+ cells and 242 taste buds in vehicle mice and 237 YFP+ cells and 245 taste buds in cabozantinib mice. Unpaired t-test performed for all quantifications. Mean+/-SEM.

In FFP taste buds, cabozantinib also had no impact on TBC survival as the number of *Kit*-YFP$^+$ cells was unchanged (**Figure S8A-B**). However, *Kit*-YFP was expressed in different TBC subpopulations in FFP compared to CVP taste buds. As in the CVP, almost all *Kit*-YFP$^+$ cells were PLCβ2$^+$ (**Figure S8C-D**). But in contrast to the CVP, ~60% of these cells were GUST$^+$ type II cells (including ~30% that were *Tas1r2*$^+$sweet cells) while ~40% of *Kit*-YFP$^+$ cells were GUST$^-$ salt cells (**Figure S8E-H**). Regardless, drug treatment did not change the percentage of *Kit*-YFP$^+$ cells expressing PLCβ2, GUST or *Tas1r2* (**Figure S8C-H**). Therefore, even though *Kit* is expressed by different PLCβ2$^+$ type II subtypes in CVP versus FFP, cabozantinib did not cause death or transdifferentiation of *Kit*-descendent TBCs in either taste field.

Cabozantinib alters the differentiation of PLCβ2$^+$ TBC subtypes

We next asked if TKI treatment altered the fate of differentiating TBCs. Sonic Hedgehog (SHH) marks post-mitotic taste precursor cells that differentiate into each of the TBC types. Precursor cells enter taste buds and express *Shh* transiently (for ~24 hrs), then differentiate into TBCs within 3 days [60, 61]. We thus employed *Shh*$^{CreER+/}$*;Rosa26*$^{tdTomato/+}$ mice to track the fate of new TBCs differentiating during drug treatment (**Figure 4A**).

In the CVP, the number of *Shh*-Tomato$^+$ TBCs was unaffected by TKI treatment, indicating cabozantinib does not impede overall differentiation of TBCs from *Shh*$^+$ precursor cells (**Figure 4B-C**). Cabozantinib also did not affect differentiation of type II TBCs broadly, as ~30% of *Shh*-Tomato$^+$ cells were PLCβ2$^+$ regardless of treatment (**Figures 4D-E**). Since cabozantinib reduced *Tas1r2*$^+$ cells with a commensurate increase in GUST$^+$ bitter/umami cells (see **Figure 2**), we hypothesized that TKI treatment would shift the fate of newly generated type II TBCs from sweet to bitter/umami fate. Consistent with this prediction, cabozantinib significantly increased the percentage of newly differentiated type II cells (Shh-Tomato$^+$/PLCβ2$^+$) that were GUST$^+$ bitter/umami cells and significantly decreased the percentage that were GUST$^-$ (**Figure 4F-I**) and *Tas1r2*$^+$ (**Figure 4H-I**). In sum, these data indicate that cabozantinib does not affect differentiation of type II cells in general, but rather prevents differentiation of new *Tas1r2*$^+$ /GUST$^-$ sweet cells, instead biasing new type II cells toward a GUST$^+$ bitter/umami fate. Finally, these results explain why cabozantinib has a greater effect with prolonged dosing (see **Figure 2**), as more TBCs are replaced over time with altered proportions of newly differentiated type II TBC subtypes.

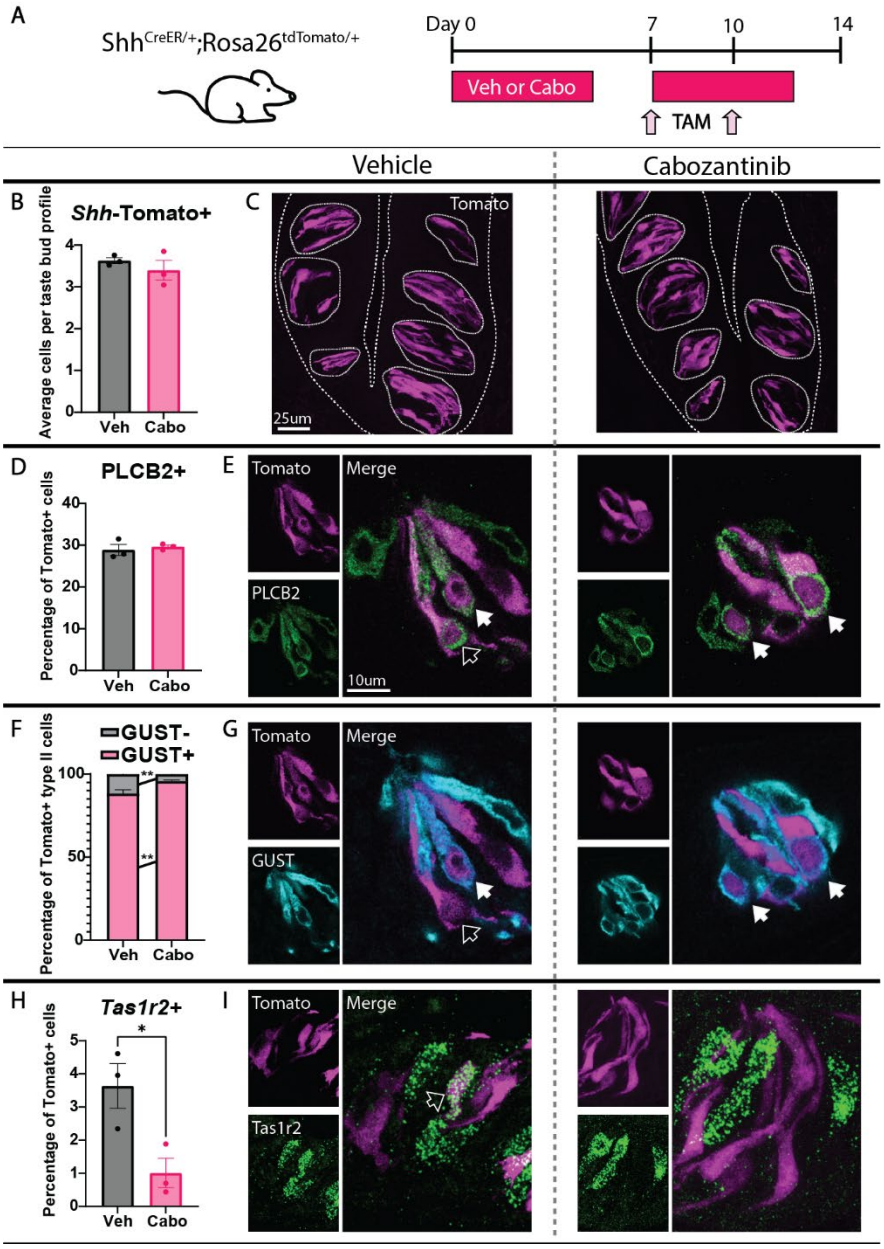

Figure 4: Cabozantinib shifts proportions of differentiating type II TBC subtypes in CVP taste buds. (**A**) *Shh*$^{CreER/+}$;*Rosa26*$^{tdTomato/+}$ mice were treated with vehicle or cabozantinib 5 days per week for 14 days and dosed with tamoxifen on days 7 and 10 to label *Shh*+ taste precursor cells. (**B**) The number of *Shh*-Tomato+ cells per taste bud profile was unaltered by cabozantinib treatment. (**C**) Compressed confocal z-stacks of *Shh*-Tomato+ TBCs in taste buds from vehicle- vs cabozantinib-treated CVPs. Coarse dashed lines delineate basement membrane and apical epithelial surface, fine dashed lines encircle individual taste buds. (**D-I**) The percentage of *Shh*-Tomato+ cells (magenta in all panels) co-expressing PLCβ2 did not change (**D-E, green in E,** optical section). The percentage of Tomato+/PLCβ2+ cells expressing GUST significantly increased, while the GUST^{neg} percentage significantly decreased (**F-G, cyan in G,** optical section). The percentage of *Shh*-Tomato+ cells expressing *Tas1r2* was significantly decreased (**H-I, green in I,** compressed z-stacks). Empty arrowheads in E, G and I indicate double-labeled cells, white arrowheads in E and G indicate triple-labeled cells. In panels D and F, values were

calculated across 874 Tomato+ cells and 218 taste buds in vehicle mice and 792 Tomato+ cells and 220 taste buds in cabozantinib mice. In panel H, values were calculated across 526 Tomato+ cells and 225 taste buds in vehicle mice and 408 Tomato+ cells and 233 taste buds in cabozantinib mice. Unpaired t-test performed for panels B, D and H. Two-way ANOVA with Sidak's multiple comparisons test performed for panel F. Mean +/- SEM (* $p \leq 0.05$, ** $p \leq 0.01$).

We also assessed the fate of newly generated TBCs in FFP taste buds. As in the CVP, drug treatment did not affect differentiation of *Shh*-Tomato$^+$ cells or the percentage of *Shh*-Tomato$^+$ cells differentiating as PLCβ2$^+$ type II TBCs (**Figure S9A-D**). Instead, cabozantinib significantly increased the percentage of *Shh*-Tomato$^+$/PLCβ2$^+$ cells that were GUST$^+$ and decreased the percentage that were GUST$^-$ (salt-sensing) (**Figure S9E-F**). Since differentiation of *Tas1r2*$^+$/GUST$^+$ sweet cells was unchanged (**Figure S9G-H**), the increase in *Shh*-Tomato$^+$/GUST$^+$ TBCs must reflect an increase in differentiated bitter/umami type II cells at the expense of GUST$^-$ salt-sensing TBCs. Thus, in both CVP and FFP taste buds, cabozantinib alters the fate of newly generated PLCβ2$^+$ TBC subtypes.

Cabozantinib impacts taste behavioral preferences of mice.

We next asked, because sweet TBCs in the CVP were diminished by TKI treatment, if sweet taste function was affected. To test this, we performed two behavioral assays: (1) a two-bottle taste preference test, and (2) a brief-access taste test. We treated mice with vehicle or cabozantinib and performed behavioral testing during the fourth week (**Figure 5A**). Mice naturally prefer sweet [62], and when presented a choice will consume/lick more sweet solution than water when sweet is detected above threshold. In two-bottle tests, neither vehicle- nor cabozantinib-treated mice preferred sweet solution at low concentrations of the non-nutritive sweetener SC45647 [63]. However, at 100μM, control mice strongly preferred SC45647, while TKI-treated mice drank equal volumes of sweetener and water, indicating no sweet preference (**Figure 5B**). Importantly, the total volume of solution consumed was not altered by drug treatment, although control mice drank significantly more 100μM SC45647, likely driven by strong preference for the sweet solution (**Figure S10A**).

We also used a brief-access paradigm in Davis Rig lickometers [64] to assess taste behavior. This apparatus allows rapid testing of multiple concentrations of tastant in a 30-minute period. Moreover, limited access tests avoid post-ingestive effects that can influence taste behavior [65]. As with two-bottle testing, cabozantinib did not alter important metrics of drinking behavior associated with participation or thirst (**Figure S10B-G**). Also consistent with 2-bottle results, control mice strongly preferred SC45647, while TKI-treated mice showed no preference for the non-nutritive sweetener (**Figure 5C**). These data indicate that cabozantinib decreases behavioral preference for sweet, consistent with histological finding of reduced sweet TBCs in CVP taste buds.

Since cabozantinib increased the number of bitter/umami type II cells in both FFP and CVP taste buds, we also tested whether TKI treatment impacted bitter taste function. As bitter is aversive to mice, we hypothesized that the drug-induced increase in GUST$^+$ cells would lower the threshold concentration for avoidance of bitter solution. However, both vehicle and cabozantinib-treated mice had comparable behavioral avoidance of quinine (**Figure 5D**). We further tested sour taste, which is mediated in part by type III TBCs [1]. Avoidance of citric acid did not differ with treatment, consistent with our finding that cabozantinib did not impact type III

cells (**Figure 5E**). Thus, cabozantinib does not affect taste preference for either bitter or sour but does blunt sweet taste preference.

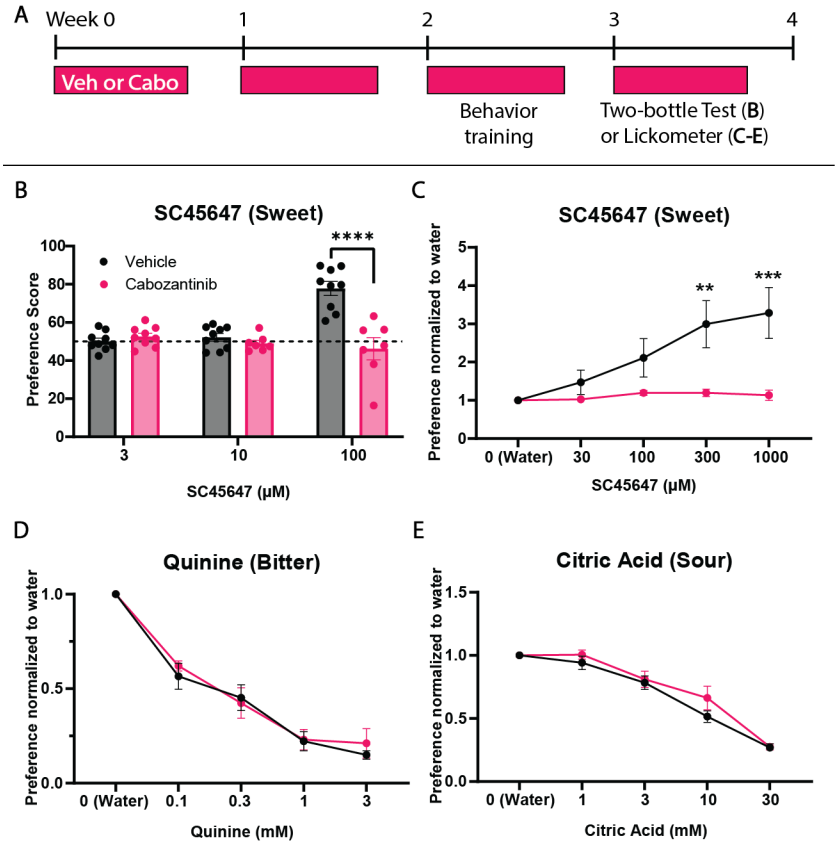

Figure 5: Sweet taste preference is blunted by cabozantinib. (**A**) Mice treated with vehicle or cabozantinib 5 days per week for 4 weeks underwent behavioral assay training in week 3, and taste behavior testing in week four. (**B**) In a two-bottle taste test, only control mice preferred sweet solution at high SC45647 concentration (N= 9 control and 7 TKI mice). Preference score = volume of SC45647 consumed / total volume of water and SC45647 consumed. Dotted line at 50 = no preference. (**C**) Brief access lickometer testing shows control mice prefer SC45647 at progressively higher concentrations while TKI-treated mice have no preference for SC45647 over water (N= 9 control and 9 TKI mice). Lickometer responses for quinine (**D**) and citric acid (**E**) were unaltered by TKI treatment (N= 9 control and 9 TKI mice). Preference = average licks for each concentration of each tastant / average licks for water. All data were analyzed using Two-way ANOVA with Sidak's multiple comparisons test. Mean +/- SEM (** $p \leq 0.01$, *** $p \leq 0.001$, **** $p \leq 0.0001$).

Conditional deletion of *Kit* results in loss of sweet TBCs in CVP and a fate shift in FFP.

Three lines of evidence suggested that inhibition of the off-target RTK KIT may underlie the differences in TBC differentiation caused by cabozantinib. In addition to intended targets VEGFRs and PDGFRβ, KIT is inhibited by all three TKIs tested [19-21]. Further, mice treated with cabozantinib developed fur depigmentation (**Figure S11**), a physiological readout of KIT inhibition in mice and humans [66]. Finally, *Kit* is expressed in differentiated sweet cells in the CVP and lineage traces into all type II cell subtypes in both taste fields, suggesting these lineages

may be directly sensitive to KIT inhibition (see **Figures 3, S7, S8**). The POU2F3 transcription factor is expressed in all type II cells and is required for their differentiation [67]. Thus, we combined the *Pou2F3*^{CreER} allele [68] with a novel floxed *Kit* allele (*Kit*^{ten}) wherein LoxP sites flank exon 10 that encodes the transmembrane domain of KIT protein (Lara et al. 2025, under revision). To delete *Kit* in the type II TBC lineage, *Pou2F3*$^{CreER/+}$*;Kit*$^{fl/fl}$ mice were dosed with tamoxifen or corn oil every other day for 2 weeks (**Figure 6A**).

Cre induction abolished KIT expression in CVP epithelium, indicating efficient *Kit* deletion (**Figures 6B-C**). As in TKI-treated mice (see **Figure 2**), *Kit* deletion did not affect the number of type II or type III cells (**Figure 6D-G**), but as with drug treatment, significantly fewer *Tas1r2*$^{+}$ sweet cells were detected (**Figure 6H-I**). Since sweet cells were reduced but not lost, this is consistent with a requirement of KIT in regulating differentiation of new sweet cells but not their maintenance (see **Figures 3-4**). Two weeks after Kit deletion, however, GUST^{+} cell number was unchanged (**Figure 6J-K**). This is somewhat consistent with results after 2 weeks of cabozantinib, where GUST^{+} cell number trended upward, but not significantly (see **Figure 2L**). Longer-term *Kit* knockout may result in increased GUST^{+} cells, as seen with 4 weeks of TKI. Alternatively, the increase in GUST^{+} type II cells observed in cabozantinib-treated mice may be independent of *Kit*.

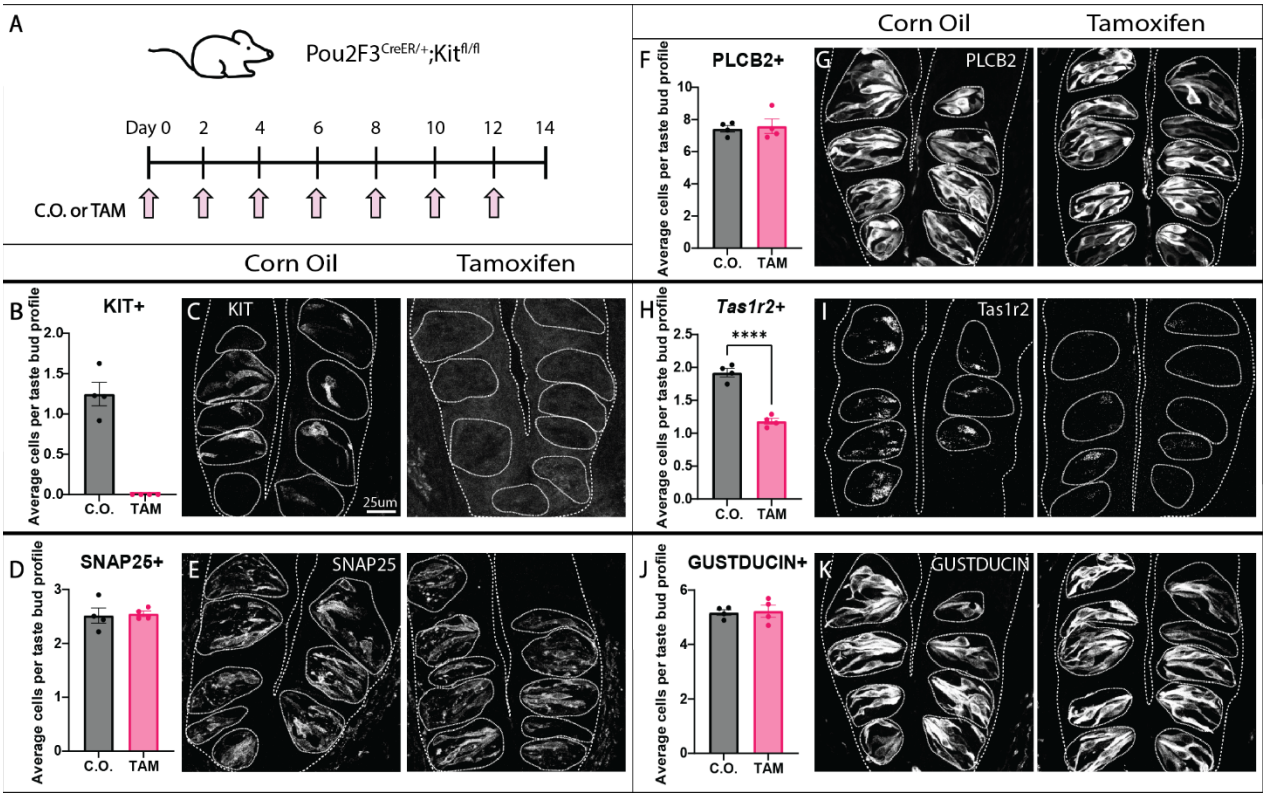

Figure 6: Conditional *Kit* knockout in the type II TBC lineage decreased sweet cells in CVP taste buds. (**A**) *Pou2F3*$^{CreER/+}$*;Kit*$^{fl/fl}$ mice were gavaged with corn oil or tamoxifen every other day for 14 days. (**B-K**) Quantification of stained cells per taste bud profile with corresponding representative images for KIT-IF (**B-C**), SNAP25-IF (**D-E**), PLCβ2-IF (**F-G**), *Tas1r2* HCR *in situ* hybridization (**H-I**) and GUSTDUCIN-IF (**J-K**). Representative images are compressed confocal z-stacks. Coarse dashed lines delineate basement membrane and apical epithelial surface, fine dashed lines encircle individual taste buds. Scale bar in C applies to E, G, I and K.

In all histograms, each dot represents the average TBC tally from each mouse (N=4 per condition, ~80 taste buds/mouse). Unpaired t-test performed on all quantifications. Mean+/-SEM (**** $p \leq 0.0001$).

In FFP taste buds, POU2F3 is expressed by all PLCβ2$^+$ cells, including sweet, bitter, and umami type II cells, and by PLCβ2$^+$ salt-sensing taste cells [34]. As in CVP, *Kit* KO in *Pou2F3*$^+$ cells efficiently ablated *Kit* in FFP taste buds. (**Figure S12A-B**). As with drug treatment, conditional deletion of *Kit* did not affect the total number of PLCβ2$^+$ or SNAP25$^+$ cells (**Figure S12C-D, G-H**), nor were *Tas1r2*$^+$ sweet cells affected (**Figure S12E-F**). Consistent with the fate shift induced by cabozantinib in FFP, GUST$^+$ bitter/umami cells increased and GUST$^-$ salt cells decreased upon *Kit* deletion (**Figure S12I-L**). Thus, *Kit* knockout phenocopies fate changes caused by TKI treatment in both CVP and FFP taste buds, suggesting the impacts of cabozantinib on type II TBC fate are due to KIT inhibition.

Discussion

Many cancer drugs have the unintended side effect of perturbing taste. Since the rapid turnover of taste buds relies upon proliferating progenitors, therapies targeting proliferating cells are especially harmful to the taste system. For example, targeted head and neck irradiation, as well as anti-mitotic chemotherapies, are cytotoxic to taste progenitors and disrupt TBC renewal [69-72]. However, we find that 3 anti-angiogenic TKIs used to treat kidney metastases do not affect taste progenitor proliferation or survival when tested in lingual organoid cultures. Disrupting taste cell differentiation can also grossly disrupt TBC renewal. Targeted drugs that inhibit SHH signaling, which is required for differentiation of new TBCs, prevent differentiation of new taste cells and thus lead to progressive taste bud degeneration as older cells are lost and not replaced [73-79] (but see [77, 79]). TKI treatment, however, also did not cause large-scale disruption of TBC differentiation *in vivo* or *in vitro*. Instead, we find that differentiation of type II TBC subtypes was dysregulated by anti-angiogenic drugs. In the CVP, cabozantinib decreased sweet type II cells and increased bitter/umami type II cells, while in FFP taste buds, sweet cells were not affected by TKI treatment. Instead, cabozantinib decreased the number of salt cells with an increase in bitter/umami cells. Although multiple type II subtypes were altered by drug treatment, only sweet taste behavior was impacted. In the CVP and FFP, these shifts in cell fate were largely recapitulated by deletion of *Kit* in the type II TBC lineage, suggesting that the impact of TKIs on type II TBC fate is at least partially due to KIT inhibition.

Lineage dynamics of taste renewal

SHH$^+$ taste precursor cells differentiate into all TBC types [60]. However, it is not known whether these cells differentiate directly into TBCs or if further intermediate cell states exist wherein additional lineage decisions are made. *Ascl1* is expressed in type III TBCs and a subset of *Shh*+ precursors [80, 81], and is required for type III cell production. Lineage tracing of *Ascl1*$^+$ cells labels primarily type III cells and a limited number of type II cells, suggesting *Shh*$^+$ precursors co-expressing *Ascl1* produce both TBC types but are biased toward type III fate [82, 83]. In contrast, *Pou2F3* is expressed by some precursor cells and type II TBCs, and is necessary for type II cell differentiation. *Pou2F3* knockout mice lose type II cells with a corresponding increase in type III cells [67]. Altogether, these studies suggest a model where precursor cells become progressively lineage restricted by *Ascl1* and *Pou2F3* expression. However, where in the lineage cells acquire type II TBC subtype fates is unknown. Since cabozantinib did not alter

differentiation of type II or type III cells but rather shifted the fate of type II TBC subtypes, we propose that *Shh*$^+$ descendent cells are first specified into ASCL1$^+$ or POU2F3$^+$ precursors, and type II subtype decisions are made subsequently in the POU2F3$^+$ lineage. Since FFP salt cells also depend on POU2F3 for differentiation [34], and since cabozantinib affected the differentiation of salt cells, our data support published findings that salt cells and type II cells arise from a common POU2F3$^+$ precursor population in FFP taste buds [34]. Hence, we hypothesize that TKIs dysregulate type II TBC subtype differentiation in POU2F3$^+$ lineage-restricted precursors, driving a fate shift toward bitter/umami subtypes vs sweet or salt type II TBCs in CVP and FFP, respectively.

KIT regulates type II TBC subtype differentiation.

In the CVP, KIT is expressed by sweet cells, while *Kit* lineage tracing revealed *Kit*-YFP in both sweet and a small proportion of bitter/umami type II TBCs. Similarly, *Kit* lineage trace was observed in sweet, bitter/umami and salt TBCs in FFP. Together, these lineage labeling results suggest that KIT is expressed in type II precursor cells, and conditional knockout in POU2F3$^+$ cells indicates that KIT is required for production of the correct proportions of type II TBC subtypes. The impact of Kit deletion was largely comparable to cabozantinib treatment; both genetic and pharmacologic approaches led to sweet cell loss in the CVP, while in the FFP, salt cells were lost with an increase in bitter/umami cells.

However, increases in bitter/umami cells in the CVP observed after cabozantinib treatment were not seen with *Kit* KO. This may be due to the shorter duration of *Kit* knockout experiments (2 weeks); if so, bitter/umami cells would be expected to increase after 4 weeks. Alternatively, the drug-induced increase in bitter/umami cells may be independent of KIT inhibition. Cabozantinib inhibits many off-target RTKs, including MET, RET, AXL, FLT3 and TEK [19-21]. Additionally, some TKIs inhibit these off-target RTKs without inhibiting KIT, and these drugs are nonetheless linked to dysgeusia [10]. Therefore, one or more of these RTKs may regulate the renewal of bitter/umami type II cells independently of sweet type II cell differentiation, and independently of KIT.

Given both *Kit* knockout and cabozantinib affect differentiation of PLCβ2$^+$ TBC subtypes, we posit that KIT signaling governs differentiation of type II TBCs. KIT regulates differentiation of multiple cell types in other systems, including T-cells [84], cardiomyocytes [85], spermatogonia [86], and melanocytes [87]. Additionally, a complementary paper using *Pou2F3*$^{CreER/+}$;*Kit*$^{fl/fl}$ mice identified KIT as a regulator of intestinal tuft cell hyperplasia following helminth infection (Lara et al. 2025, under revision). In this context, KIT is required for the proliferation and/or differentiation of tuft cells during a type II immune response. Tuft cells also require POU2F3 for their generation [88], suggesting a shared requirement of KIT signaling in regulating the differentiation of POU2F3-dependent cells throughout multiple epithelial systems.

Mechanisms of behavioral taste alterations

Cabozantinib and *Kit* knockout impact fate selection of type II TBCs in CVP and FFP, but shifts in subtype fates differ between the two taste fields. These discordant changes in different taste papillae may contribute to TKI-induced dysgeusia. In rodents it is well established that FFP taste buds in the anterior tongue are more highly tuned to sweet, while posterior taste buds are more sensitive to bitter [43, 44]. Thus, we were surprised when cabozantinib had no impact on sweet cells in FFP despite the loss of behavioral preference for sweet. Instead, sweet

cell loss was evident only in CVP taste buds. Incongruent input from these two taste fields may change how taste stimuli are perceived. Alternatively, sweet taste behavioral responses may depend on proper sweet cell renewal in both FFP and CVP, as normal sweet cell number in FFP did not appear to compensate for reduced sweet TBCs in the CVP.

Sweet taste is highly appetitive and signals caloric and nutritious food [62]. Maintaining a minimum number/ratio of sweet cells in taste buds may be required to properly convey appetitive quality. Cabozantinib decreased, but did not eliminate, sweet cells from CVP taste buds, yet mice lost behavioral responses to sweet. TKI treatment may have therefore decreased the number of sweet cells below a threshold for adequate sweet detection. Alternatively, CVP taste buds have been proposed to regulate a binary accept/reject response rather than fine taste discrimination [89-91], and thus diminished sweet cell number in CVP taste buds may decrease the acceptance of sweet tastants. KIT inhibition may also affect nerve transduction, as KIT regulates synaptic inhibition between pre- and post-synaptic neurons in cerebellum [92, 93]. Thus, KIT function may regulate transmission of taste information from KIT^+ cells to gustatory nerve fibers, which could explain the complete loss of sweet taste preference in cabozantinib-treated mice. Behavioral preferences for bitter and sour tastants, on the other hand, were unaffected by TKI treatment. Since bitter cells in both CVP and FFP taste buds express GUST [50, 59], we expected their increase to likewise increase sensitivity to bitter. However, behavioral sensitivity to bitter compounds may already be maximal. Many plants, fungi, and animals produce toxic or poisonous substances to deter predation; these are almost always bitter. Thus, the taste system has evolved to be highly sensitive to bitter substances [62], such that here, small increases in bitter cells would have little functional consequence. Overall, our data suggest that loss of sweet taste function is a primary cause of TKI-induced dysgeusia. Intriguingly, sweet taste has been reported to be the most commonly affected taste modality in patients treated with TKIs for gastrointestinal stromal tumors [94].

Limitations and future directions

A potential limitation of this study is that while TKI treatment decreased the number of salt-sensing type II cells in FFP taste buds, we did not test salt behavior in TKI-treated mice. FFP salt TBCs mediate detection of low, appetitive concentrations of salt [34]. Practically, motivating mice to prefer such low concentrations requires dietary salt depletion that may not be well tolerated by TKI-treated mice [32]. Additionally, while the taste system of mice is broadly similar to that of humans [95], we can only speculate that humans experience similar cell type shifts and changes in taste preferences. This limitation could be addressed in the future by collecting taste bud biopsies from TKI-treated patients to investigate whether cellular changes are similar to those observed in mice, and by performing psychophysical taste testing for individual tastants [96] in patients experiencing dysgeusia.

In closing, given the importance of sweet cells in the maintenance of sweet taste preference, and KIT's role in regulating sweet cell renewal in CVP taste buds, we propose that KIT inhibition contributes to TKI-induced dysgeusia. In addition to the three TKIs tested here, KIT is an off-target RTK of seven anti-angiogenic TKIs currently used in clinical practice [19, 97, 98]. Thus, KIT inhibition may underlie dysgeusia in this large class of chemotherapeutics. For drugs used to treat mRCC, KIT is not an intended target, as therapeutic efficacy relies primarily on VEGFR and PDGFRβ inhibition [98]. Developing alternatives that maintain inhibition of these targets without inhibiting KIT could alleviate dysgeusia while maintaining

efficacy in treating mRCC. There are also cancers in which oncogenic KIT mutations drive tumorigenesis, such as gastrointestinal stromal tumors, melanomas, small cell lung cancer and many leukemias [99]. Unfortunately, treating these cancers requires KIT inhibition and therefore dysgeusia is likely unavoidable. Developing targeted therapies that specifically inhibit mutated KIT without inhibiting wild-type KIT may mitigate dysgeusia in these cases. By establishing KIT as a regulator of type II TBC subtype renewal and showing that *Kit* knockout in part underpins the response to TKI treatment, we have provided a promising candidate for future mitigation strategies.

Materials and Methods

Animals

Commercially available mice were obtained from the Jackson Laboratory ($Lgr5^{EGFP\text{-}IRES\text{-}CreERT2}$, 008875; $Shh^{CReERT2}$; 005623, $Rosa26^{TdTomato}$; 007909, $Rosa26^{YFP}$; 006148, $Pou2F3^{CreERT2\text{-}IRES\text{-}eGFP}$; 037511). $Kit^{CreER/+}$;$Rosa26^{YFP/YFP}$ mice were a gift from Stephen W. Santoro, University of Colorado Anschutz Medical Campus, Aurora CO (originally reported [100]). $Pou2F3^{CreERT2\text{-}IRES\text{-}eGFP\ /+}$;$Kit^{fl/fl}$ mice were a gift from the Jakob von Moltke, University of Washington, Seattle WA (Lara et al. 2025, in revision). Mice were maintained in an AAALAC-accredited facility in compliance with the Guide for Care and Use of Laboratory Animals, Animal Welfare Act, and Public Health Service Policy. Male and female adult mice between 8-20 weeks were used. Procedures were approved by the Institutional Animal Care and Use Committee at the University of Colorado Anschutz Medical Campus.

Administration of drugs

Cabozantinib malate (XL 184, SelleckChem) was suspended in HPLC water at 6mg/ml with 5µl/ml 1N HCL (Fisher Chemical), sonicated for 10 min, heated at 37˚C for 15 min with vortexing, and sonicated for another 10 min. Adult mice on mixed background were dosed with 60mg/kg cabozantinib or vehicle via oral gavage. Mice were weighed daily to monitor health.

Tamoxifen: Tamoxifen (Sigma-Aldrich) was suspended in corn oil + 10% ETOH at 10mg/ml. Adult mice were gavaged with 50 mg/kg ($Shh^{CreER/+}$;$Rosa^{26tdTomato/+}$) or 100 mg/kg ($Kit^{CreER/+}$;$Rosa26^{YFP/YFP}$ and $Pou2F3^{CreER/+}$;$Kit^{fl/fl}$). Daily cage changes were preformed for 7 days after final tamoxifen dose or until mice were harvested, whichever came first.

Behavioral Assays

Two-bottle taste preference test: Preference for SC45647 was tested in a 48 hr two-bottle behavioral assay [65]. Mice were individually housed in regular ventilated cages with *ad libitum* chow. Graduated bottles were created from cut plastic serological pipettes fitted with a sipper tube on one end and a rubber stopper on the other. Mice were trained for 4 days; first with deionized water in one of 2 bottles, and positions switched after 24 hrs. In the second 2 days, mice had access to water in both bottles. To test sweet taste preference, mice had one bottle of water and one bottle of SC45647 (3 µM in deionized water) for 48 hrs; the volume consumed was measured at 24 hrs, bottles refilled as necessary, and left-right position switched to control for side preference. Sweet preference ratio was calculated by dividing the volume of SC45647 consumed by the sum of the volume of water and SC45647 consumed over 48 hrs. This was repeated for 10 µM and 100 µM SC45647.

Brief Access Test (Lickometer): Three Davis Rig MS-160 lickometers (DiLog Instruments, Inc., Tallahassee, FL, USA) were used to test taste perception of vehicle- and cabozantinib-treated mice. Detailed protocol and operating procedures have been described fully [65]. During the last 2 weeks of drug or vehicle treatment, mice were trained and tested in one of three lickometers randomly assigned each day. Chamber areas were reduced by half to reduce distraction from surroundings and exploration. Training and test sessions were limited to 30 min. During brief-access testing a shutter opens to give mice access to a bottle of tastant for 5 sec (counted from first lick), the shutter closes for 7.5 sec, and the next bottle is moved into position via an automated mobile rack for the next 5 sec trial. Mice were water deprived for 23.5 hrs prior to training or testing to motivate drinking. Mice were trained to drink water in the lickometer for 4 consecutive days. For 2 days, the shutter was open and water available for 30 min. On days 3 and 4, two bottles of water were alternately presented for 5 sec each for 30 min. After 2 days of recovery, mice had a final day of training with two alternating bottles of water. Once trained, mice were tested for behavioral taste preference for 4 days. For each cabozantinib vs vehicle experiment, only 2 of a total of 3 tastants were assayed, each for 2 days. These included: Sweet - SC45647 (30, 100, 300 and 1000 µM), Bitter - quinine (0.1, 0.3, 1 and 3 mM) and Sour - citric acid (1, 3, 10 and 30 mM). All solutions were made in deionized water. Each test session consisted of up to eight trial blocks (each block comprised five presentations in random order - water and 4 concentrations of one tastant). For sweet SC45647, the first block was not included in our analysis as a thirst-induced high motivational state during the first block may drive maximal licking for all solutions [65]. Mouse thirst for all tastants was calculated from the total licks across the first block averaged across the two testing days. Results of behavior tests are expressed as the lick ratio (average licks to tastant/average licks to water).

Tissue Preparation

Mice were euthanized by CO_2 asphyxiation. Tongues were dissected from the lower jaw, incubated for 3 hrs at 4°C in 4% paraformaldehyde (PFA) in 0.1 M phosphate buffer (PB), and placed in sucrose (20% in 0.1 M PB) overnight at 4°C. Samples were embedded in OCT Compound (Tissue-Tek), 12 µm cryosections collected on SuperFrost Plus slides (Thermo Fisher Scientific) and stored at −80°C. For the CVP, 6 sets of 9 sections were collected, while for the FFP, 6 sets of 16 sections were collected.

Immunofluorescence

Tissue sections: Sections were washed in 0.1 M PBS, incubated in blocking solution (BS: 5% normal goat or donkey serum, 1% bovine serum albumin, 0.3% Triton X-100 in 0.1 M PBS at pH 7.3) for 1.5 hrs RT followed by primary antibodies (Table S2) diluted in BS overnight at 4°C. Sections were rinsed in PBS+0.1% Triton, incubated for 1 hr at RT in secondary antibodies in BS, followed by DAPI nuclear counterstaining (Invitrogen; 1:10,000). Slides were cover-slipped with ProLong Gold (Thermo Fisher Scientific).

Organoids: Organoids were generated from taste progenitor cells obtained via FACS of dissociated CVP epithelia from *Lgr5*$^{EGFP\text{-}IRES\text{-}CreERT2}$ mice following our published protocol [45]. To harvest, organoids were incubated in Cell Recovery Solution (Corning) at 4°C, washed in 0.1 M PBS, fixed in 4% PFA and stored at 4°C in PBS with 1% BSA. For immunofluorescence, organoids were incubated in BS (2 hrs), then with primary antibodies (Table S2) in BS for 3

nights at 4°C, washed with PBS+0.2% Triton and incubated with secondary antibodies in BS overnight at 4°C. Organoid nuclei were counterstained with DAPI, washed with 0.1 M PB and mounted on SuperFrost Plus slides in Fluoromount (Southern Biotech).

Hybridization chain reaction RNA-fluorescence *in situ* hybridization

Molecular Instruments designed and produced probes against *Tas1r2* (NM_031873.1), *Kit* (NM_001122733.1) and *Trpm5* (NM_020277.2). Methods were adapted from the manufacturer's protocol. Fixed frozen sections were incubated in 4% PFA for 10 min at RT, washed with 0.1 M PBS and incubated in 2 µg/ml Proteinase K for 2 min (CVP) or 5 min (FFP) at RT. Sections were incubated in triethanolamine solution, 12 M HCl and acetic anhydride in DEPC-treated water for 10 min at RT, washed with PBS, incubated in hybridization buffer for 45 min at 37°C, and then with 1.2 pmol (CVP) or 1.5 pmol (FFP) probe in hybridization buffer overnight at 37°C. Sections were washed with 75% wash buffer/25% 5× SSCT (20× SSC and 10% Tween20, ultrapure water), 50% wash buffer/50% 5× SSCT, 25% wash buffer/75% 5× SSCT, and 100% 5× SSCT, each for 20 min at 37°C, then with 100% 5× SSCT for 20 min at RT. Sections were incubated in amplification buffer for 1 hr, then in denatured hairpin solution (6 pmol hairpin 1 and 2 in amplification buffer) overnight. Slides were washed with 5× SSCT, nuclei counterstained with DAPI, washed with 0.1 M PB and cover-slipped with ProLong Gold.

Organoid Derivation

Organoids were derived according to our protocol [45]. For each experiment, organoids were derived from CVP epithelium from 3-6 *Lgr5*$^{EGFP\text{-}IRES\text{-}CreERT2}$ mice aged 8-20 weeks. Briefly, collagenase (2 mg/ml) and dispase (5 mg/ml) in phosphate-buffered saline (PBS) were injected around the CVP, the epithelium peeled and dissociated for 45 min in collagenase (2 mg/ml), dispase (5 mg/ml) and elastase (2 mg/ml) at 37°C. Cells were centrifuged (320 ***g*** at 4°C), the pellet resuspended in FACS buffer [1 mM EDTA, 25 mM HEPES (pH 7.0), 1% FBS, 1×Ca^{2+}/Mg^{2+}-free dPBS], passed through a 30 µm cell strainer, stained with DAPI (Thermo Fisher Scientific) and subjected to FACS on a MoFlo XDP100 (Cytomation). Debris and doublets were gated out via side-scatter (FSC and SSC-width, respectively), live (DAPI-) cells were enriched, and the gating of GFP^+ signal was determined relative to background fluorescence of epithelial cells from a wild-type control mouse processed in parallel (see [45] for gating strategy). Only *Lgr5*-GFP^+ cells were collected. Sorted GFP^+ cells were plated in 48-well plates at 200 cells/well in 15 µl Matrigel and grown in WENR+AS media to support growth (days 0-6) and WENR media to promote TBC differentiation (days 6-12). WENR: 50% WRN (WNT/RSPO/Noggin)-conditioned media [101] plus 1× Glutamax (Gibco), 1× HEPES (Gibco), 1× penicillin-streptomycin (Gibco), 1× B27 supplement (Gibco), 1× gentamicin (Gibco), 1× primocin (InvivoGen), 25 ng/ml murine Noggin (Peprotech), 50 ng/ml murine EGF (Peprotech), 1 mM nicotinamide (Sigma), and 1 mM N-acetyl-L-cysteine (Sigma). WENR+AS: WENR plus 500 nM A83-01 (Sigma) and 0.4 µM SB202190 (R&D Systems). Y27632 (10 µm; Stemgent) was added on days 0-2 to promote cell survival.

<u>Drug treatment</u>: cabozantinib (SelleckChem; S4001), axitinib (SelleckChem; S1005), sunitinib (SelleckChem; S7781), and paclitaxel (SelleckChem; S1150) were dissolved in DMSO to a stock concentration of 50µM, and diluted in organoid media (WENR+AS or WENR depending on the experiment) to a final concentration of 50nM or 100nM. For controls, the same volume of DMSO was added to organoid media. Medium was changed every 2 days.

Quantitative RT-PCR

Organoids were harvested as described [45]. Briefly, plates were placed on ice for 30 min and organoids freed from Matrigel by scratching with a pipet tip. Organoid samples were centrifuged and resuspended in RLT buffer (Qiagen) with β-mercaptoethanol. RNA was extracted using a RNeasy Micro Kit (Qiagen), quantified via Nanodrop (Thermo Fisher Scientific) and reverse transcribed with an iScript cDNA synthesis kit (Bio-Rad). Power SYBR Green PCR Master Mix (Applied Biosystems) was used for qPCR reactions on a StepOne Plus Real-Time PCR System (Applied Biosystems, Life Technologies). Relative gene expression was assessed using the ΔΔCT method [102], with *Rpl19* as the housekeeping gene. Primers are listed in **Table S1**. Organoids from three wells of a 48-well plate were pooled per RNA sample and three samples were collected per experiment for RT-qPCR.

EdU incubation, detection and quantification

Organoids were grown in 48-well plates as described above and on day 6, EdU (4mM stock in 0.9% NaCl) was added to WENR+AS media at a final concentration of 10µM for 30 min. Cultures were placed in fresh WENR+AS on ice and organoids harvested for immunofluorescence as above. A Click-it® EdU Alexa Fluor® 647 Imaging Kit (Invitrogen) was used to detect EdU signal using methods adapted from the manufacturer's protocol. Organoids were washed with PBS +0.2% Triton, washed with PBS + 0.1% BSA, then incubated in Click-it® Plus reaction cocktail for 3 hrs at RT. Organoids were washed with PBS, nuclei counterstained with DAPI, washed with 0.1 M PB and mounted on SuperFrost Plus slides in Fluoromount (Southern Biotech). Using a custom app - OrganoidAnalyzer in MATLAB 2024a (Mathworks, Natick, MA) (https://github.com/salcedoe/OrganoidAnalysis) we determined the ratio of EdU^+ pixels to total $DAPI^+$ pixels in each organoid. See supplemental materials for details.

Cell-Titer Glo® 3D

Organoids were derived and cultured as above but in opaque-walled 96-well plates at 100 cells per well in 3µl Matrigel. On day 6, plates were equilibrated to RT for 30 min, after which an equal volume of Cell-Titer Glo® 3D reagent (Promega) was added to cultures (150 µl WENR+AS with drugs or DMSO + 150 µl reagent in each well). Plates were mixed on an automatic plate shaker for 5 min to induce cell lysis. Luminescence was recorded after 25 min using a Synergy H1 microplate reader (BioTek). The average luminescence across 6 wells was calculated for each condition in each biological replicate.

Image acquisition and analysis

Immunofluorescence: Tissue sections and organoids were imaged with a Leica TCS SP8 laser-scanning confocal microscope with LAS X software. *Z*-stacks of optical sections of CVP and FFP sections were acquired at 0.75 µm thickness, and organoids at 2 µm optical section thickness. For image acquisition, analysis, and cell counts using LAS X Office software, investigators were blinded to condition. For CVP, all taste buds in 5 tissue sections were counted. For FFP, all taste buds in 16 sections from the tongue tip were counted. Criteria for immunolabeled cell counts: (1) cell is immunomarker-positive; and (2) has a $DAPI^+$ nucleus. Taste buds were identified during cell counting using either PLCβ2 staining (co-staining with

GUST and YFP), KRT8 staining (co-staining with SNAP25 and KIT), or *Trpm5* HCR *in-situ* hybridization (with *Tas1r2* probe).

Taste bud area: Maximum z-stack projections of KRT8 immunofluorescence tissue sections were generated and imported into ImageJ software. A scalebar was used to set pixels/µm scale. Individual taste buds were outlined using the Freehand Selection tool, to obtain the area of each taste bud profile.

Statistical analyses

In experiments with two conditions, normally distributed data were analyzed by unpaired t-test, and Mann-Whitney U tests were used when data were not normally distributed. In experiments with more than two conditions, normally distributed data were analyzed by ordinary one- or two-way ANOVA with either Sidak's or Tukey's multiple comparisons post-hoc test. A Kruskal-Wallis comparison test was used when data were not normally distributed. All statistical analyses employed GraphPad Prism software. Data plotted throughout are depicted as Mean ± S.E.M. and significance was taken as $p<0.05$ with a confidence interval of 95%.

References

1. Liman, E.R., Y.V. Zhang, and C. Montell, *Peripheral coding of taste.* Neuron, 2014. **81**(5): p. 984-1000.
2. Gaillard, D. and L.A. Barlow, *A Mechanistic Overview of Taste Bud Maintenance and Impairment in Cancer Therapies.* Chem Senses, 2021. **46**.
3. Epstein, J.B. and A. Barasch, *Taste disorders in cancer patients: pathogenesis, and approach to assessment and management.* Oral Oncol, 2010. **46**(2): p. 77-81.
4. Sánchez-Lara, K., et al., *Influence of taste disorders on dietary behaviors in cancer patients under chemotherapy.* Nutrition journal, 2010. **9**: p. 15-15.
5. Vigarios, E., J.B. Epstein, and V. Sibaud, *Oral mucosal changes induced by anticancer targeted therapies and immune checkpoint inhibitors.* Supportive Care in Cancer, 2017. **25**(5): p. 1713-1739.
6. Kiselyov, A., K.V. Balakin, and S.E. Tkachenko, *VEGF/VEGFR signalling as a target for inhibiting angiogenesis.* Expert Opin Investig Drugs, 2007. **16**(1): p. 83-107.
7. Raica, M. and A.M. Cimpean, *Platelet-Derived Growth Factor (PDGF)/PDGF Receptors (PDGFR) Axis as Target for Antitumor and Antiangiogenic Therapy.* Pharmaceuticals (Basel), 2010. **3**(3): p. 572-599.
8. Hahn, A.W., et al., *First-line Treatment of Metastatic Renal Cell Carcinoma: A Systematic Review and Network Meta-analysis.* Eur Urol Oncol, 2019. **2**(6): p. 708-715.
9. Roberto, M., et al., *Metastatic Renal Cell Carcinoma Management: From Molecular Mechanism to Clinical Practice.* Frontiers in oncology, 2021. **11**: p. 657639-657639.
10. Hamazaki, R. and Y. Uesawa, *Characterization of Antineoplastic Agents Inducing Taste and Smell Disorders Using the FAERS Database.* Pharmaceuticals (Basel), 2024. **17**(9).
11. Strell, C., E. Rodríguez-Tomàs, and A. Östman, *Functional and clinical roles of stromal PDGF receptors in tumor biology.* Cancer Metastasis Rev, 2024. **43**(4): p. 1593-1609.
12. Koch, S., et al., *Signal transduction by vascular endothelial growth factor receptors.* Biochemical Journal, 2011. **437**(2): p. 169-183.
13. Schaum, N., et al., *Single-cell transcriptomics of 20 mouse organs creates a Tabula Muris.* Nature, 2018. **562**(7727): p. 367-372.

14. Sukumaran, S.K., et al., *Whole transcriptome profiling of taste bud cells.* Scientific Reports, 2017. **7**(1): p. 7595.
15. Ren, W., et al., *Transcriptome analyses of taste organoids reveal multiple pathways involved in taste cell generation.* Sci Rep, 2017. **7**(1): p. 4004.
16. Yamada, Y., et al., *Gene expression profiling of α-gustducin-expressing taste cells in mouse fungiform and circumvallate papillae.* Biochem Biophys Res Commun, 2021. **557**: p. 206-212.
17. Golden, E.J., et al., *Onset of taste bud cell renewal starts at birth and coincides with a shift in SHH function.* Elife, 2021. **10**.
18. Shechtman, L.A., et al., *High Sox2 expression predicts taste lineage competency of lingual progenitors in vitro.* Development, 2023. **150**(4).
19. Klaeger, S., et al., *The target landscape of clinical kinase drugs.* Science, 2017. **358**(6367).
20. Karaman, M.W., et al., *A quantitative analysis of kinase inhibitor selectivity.* Nature Biotechnology, 2008. **26**(1): p. 127-132.
21. Davis, M.I., et al., *Comprehensive analysis of kinase inhibitor selectivity.* Nature Biotechnology, 2011. **29**(11): p. 1046-1051.
22. Biggs, B.T., T. Tang, and R.F. Krimm, *Insulin-Like Growth Factors Are Expressed in the Taste System, but Do Not Maintain Adult Taste Buds.* PLoS One, 2016. **11**(2): p. e0148315.
23. Choo, E. and R. Dando, *The c-kit Receptor Tyrosine Kinase Marks Sweet or Umami Sensing T1R3 Positive Adult Taste Cells in Mice.* Chemosensory Perception, 2021. **14**(1): p. 41-46.
24. Donnelly, C.R., et al., *Biphasic functions for the GDNF-Ret signaling pathway in chemosensory neuron development and diversification.* Proc Natl Acad Sci U S A, 2018. **115**(3): p. E516-e525.
25. McLaughlin, S.K., *Erb and c-Kit receptors have distinctive patterns of expression in adult and developing taste papillae and taste buds.* J Neurosci, 2000. **20**(15): p. 5679-88.
26. Wang, K., et al., *Exploring the Role of Ccn3 in Type III Cell of Mice Taste Buds.* Journal of Neurochemistry, 2025. **169**(1): p. e16291.
27. Delay, R.J., S.D. Roper, and J.C. Kinnamon, *Ultrastructure of mouse vallate taste buds: II. Cell types and cell lineage.* Journal of Comparative Neurology, 1986. **253**(2): p. 242-252.
28. Kinnamon, J.C., D.M. Henzler, and S.M. Royer, *HVEM ultrastructural analysis of mouse fungiform taste buds, cell types, and associated synapses.* Microscopy research and technique, 1993. **26**(2): p. 142-156.
29. Finger, T.E. and W.L. Silver, *Cell biology of taste epithelium*, in *The neurobiology of taste and smell*, T.E. Finger, W.L. Silver, and D. Restrepo, Editors. 2000, Wiley-Liss: New York. p. 287-314.
30. Ohtubo, Y. and K. Yoshii, *Quantitative analysis of taste bud cell numbers in fungiform and soft palate taste buds of mice.* Brain Res, 2011. **1367**: p. 13-21.
31. Ogata, T. and Y. Ohtubo, *Quantitative Analysis of Taste Bud Cell Numbers in the Circumvallate and Foliate Taste Buds of Mice.* Chem Senses, 2020. **45**(4): p. 261-273.
32. Chandrashekar, J., et al., *The cells and peripheral representation of sodium taste in mice.* Nature, 2010. **464**(7286): p. 297-301.

33. Nomura, K., et al., *All-Electrical Ca(2+)-Independent Signal Transduction Mediates Attractive Sodium Taste in Taste Buds.* Neuron, 2020. **106**(5): p. 816-829.e6.
34. Ohmoto, M., et al., *Sodium–Taste Cells Require Skn-1a for Generation and Share Molecular Features with Sweet, Umami, and Bitter Taste Cells.* eneuro, 2020. **7**(6): p. ENEURO.0385-20.2020.
35. Beidler, L.M. and R.L. Smallman, *Renewal of cells within taste buds.* J Cell Biol, 1965. **27**(2): p. 263-72.
36. Farbman, A.I., *Fine structure of degenerating taste buds after denervation.* Development, 1969. **22**(1): p. 55-68.
37. Hamamichi, R., M. Asano-Miyoshi, and Y. Emori, *Taste bud contains both short-lived and long-lived cell populations.* Neuroscience, 2006. **141**(4): p. 2129-38.
38. Perea-Martinez, I., T. Nagai, and N. Chaudhari, *Functional cell types in taste buds have distinct longevities.* PloS one, 2013. **8**(1): p. e53399.
39. Xu, M., et al., *WNT10A mutation causes ectodermal dysplasia by impairing progenitor cell proliferation and KLF4-mediated differentiation.* Nat Commun, 2017. **8**: p. 15397.
40. Barlow, L.A., *Progress and renewal in gustation: new insights into taste bud development.* Development, 2015. **142**(21): p. 3620-9.
41. Piarowski, C.M., T.J. Isner, and L.A. Barlow, *Developing and regenerating a sense of taste*, in *Current Topics in Developmental Biology*. 2025, Academic Press.
42. Purves, D., et al., *Organization of the taste system*, in *Neuroscience, 2nd edition*. 2001, Sinauer Associates: Sunderland (MA).
43. Shingai, T. and L.M. Beidler, *Response characteristics of three taste nerves in mice.* Brain Res, 1985. **335**(2): p. 245-9.
44. Ninomiya, Y., H. Kajiura, and K. Mochizuki, *Differential taste responses of mouse chorda tympani and glossopharyngeal nerves to sugars and amino acids.* Neurosci Lett, 1993. **163**(2): p. 197-200.
45. Shechtman, L.A., et al., *Generation and Culture of Lingual Organoids Derived from Adult Mouse Taste Stem Cells.* JoVE, 2021(170): p. e62300.
46. Weaver, B.A., *How Taxol/paclitaxel kills cancer cells.* Mol Biol Cell, 2014. **25**(18): p. 2677-81.
47. Bartel, D.L., et al., *Nucleoside triphosphate diphosphohydrolase-2 is the ecto-ATPase of type I cells in taste buds.* Journal of Comparative Neurology, 2006. **497**(1): p. 1-12.
48. Rössler, P., et al., *Identification of a phospholipase C beta subtype in rat taste cells.* Eur J Cell Biol, 1998. **77**(3): p. 253-61.
49. Wilson, C.E., T.E. Finger, and S.C. Kinnamon, *Type III Cells in Anterior Taste Fields Are More Immunohistochemically Diverse Than Those of Posterior Taste Fields in Mice.* Chem Senses, 2017. **42**(9): p. 759-767.
50. Kim, M.-R., et al., *Regional expression patterns of taste receptors and gustducin in the mouse tongue.* Biochemical and Biophysical Research Communications, 2003. **312**(2): p. 500-506.
51. Wang, H., et al., *Expression of the voltage-gated potassium channel KCNQ1 in mammalian taste bud cells and the effect of its null-mutation on taste preferences.* Journal of Comparative Neurology, 2009. **512**(3): p. 384-398.
52. Iwasaki, S., H. Aoyagi, and H. Yoshizawa, *Localization of keratins 13 and 14 in the lingual mucosa of rats during the morphogenesis of circumvallate papillae.* Acta Histochem, 2011. **113**(4): p. 395-401.

53. Dvoryanchikov, G., et al., *Inward rectifier channel, ROMK, is localized to the apical tips of glial-like cells in mouse taste buds.* Journal of Comparative Neurology, 2009. **517**(1): p. 1-14.
54. Kataoka, S., et al., *The candidate sour taste receptor, PKD2L1, is expressed by type III taste cells in the mouse.* Chemical senses, 2008. **33**(3): p. 243-254.
55. Nelson, G., et al., *Mammalian sweet taste receptors.* Cell, 2001. **106**(3): p. 381-90.
56. Hirose, F., et al., *Expression of protocadherin-20 in mouse taste buds.* Sci Rep, 2020. **10**(1): p. 2051.
57. Lacy, S.A., D.R. Miles, and L.T. Nguyen, *Clinical Pharmacokinetics and Pharmacodynamics of Cabozantinib.* Clin Pharmacokinet, 2017. **56**(5): p. 477-491.
58. Yang, R., et al., *Taste cells with synapses in rat circumvallate papillae display SNAP-25-like immunoreactivity.* J Comp Neurol, 2000. **424**(2): p. 205-15.
59. Tomonari, H., et al., *Gα-gustducin Is Extensively Coexpressed with Sweet and Bitter Taste Receptors in both the Soft Palate and Fungiform Papillae but Has a Different Functional Significance.* Chemical Senses, 2011. **37**(3): p. 241-251.
60. Miura, H., et al., *Sonic hedgehog-expressing basal cells are general post-mitotic precursors of functional taste receptor cells.* Dev Dyn, 2014. **243**(10): p. 1286-97.
61. Miura, H., Y. Kusakabe, and S. Harada, *Cell lineage and differentiation in taste buds.* Archives of histology and cytology, 2006. **69**(4): p. 209-225.
62. Reed, D.R. and A. Knaapila, *Genetics of taste and smell: poisons and pleasures.* Prog Mol Biol Transl Sci, 2010. **94**: p. 213-40.
63. Nofre, C., J.M. Tinti, and F.O. Chatzapoulos, *Sweetening Agents*. 1990: United States.
64. Smith, J.C., *The history of the "Davis Rig".* Appetite, 2001. **36**(1): p. 93-98.
65. Gaillard, D. and J.M. Stratford, *Measurement of Behavioral Taste Responses in Mice: Two-Bottle Preference, Lickometer, and Conditioned Taste-Aversion Tests.* Current protocols in mouse biology, 2016. **6**(4): p. 380-407.
66. Moss, K.G., et al., *Hair depigmentation is a biological readout for pharmacological inhibition of KIT in mice and humans.* J Pharmacol Exp Ther, 2003. **307**(2): p. 476-80.
67. Matsumoto, I., et al., *Skn-1a (Pou2f3) specifies taste receptor cell lineage.* Nature neuroscience, 2011. **14**(6): p. 685-687.
68. McGinty, J.W., et al., *Tuft-Cell-Derived Leukotrienes Drive Rapid Anti-helminth Immunity in the Small Intestine but Are Dispensable for Anti-protist Immunity.* Immunity, 2020. **52**(3): p. 528-541.e7.
69. Jewkes, B.C., L.A. Barlow, and E.R. Delay, *Effect of radiation on sucrose detection thresholds of mice.* Chemical senses, 2018. **43**(1): p. 53-58.
70. Gaillard, D., et al., *Fractionated head and neck irradiation impacts taste progenitors, differentiated taste cells, and Wnt/β-catenin signaling in adult mice.* Sci Rep, 2019. **9**(1): p. 17934.
71. Mukherjee, N., et al., *Cellular mechanisms of cyclophosphamide-induced taste loss in mice.* PLoS One, 2017. **12**(9): p. e0185473.
72. Ren, W., et al., *Cisplatin attenuates taste cell homeostasis and induces inflammatory activation in the circumvallate papilla.* Theranostics, 2023. **13**(9): p. 2896-2913.
73. Castillo, D., et al., *Induction of ectopic taste buds by SHH reveals the competency and plasticity of adult lingual epithelium.* Development, 2014. **141**(15): p. 2993-3002.
74. Castillo-Azofeifa, D., et al., *Sonic hedgehog from both nerves and epithelium is a key trophic factor for taste bud maintenance.* Development, 2017. **144**(17): p. 3054-3065.

75. Liu, H.X., et al., *Multiple Shh signaling centers participate in fungiform papilla and taste bud formation and maintenance.* Dev Biol, 2013. **382**(1): p. 82-97.
76. Kumari, A., et al., *Hedgehog pathway blockade with the cancer drug LDE225 disrupts taste organs and taste sensation.* J Neurophysiol, 2015. **113**(3): p. 1034-40.
77. Kumari, A., et al., *Species generalization and differences in Hedgehog pathway regulation of fungiform and circumvallate papilla taste function and somatosensation demonstrated with sonidegib.* Sci Rep, 2018. **8**(1): p. 16150.
78. Yang, H., et al., *Vismodegib, an antagonist of hedgehog signaling, directly alters taste molecular signaling in taste buds.* Cancer Med, 2015. **4**(2): p. 245-52.
79. Lu, W.J., et al., *Neuronal delivery of Hedgehog directs spatial patterning of taste organ regeneration.* Proc Natl Acad Sci U S A, 2018. **115**(2): p. E200-e209.
80. Seta, Y., et al., *The bHLH transcription factors, Hes6 and Mash1, are expressed in distinct subsets of cells within adult mouse taste buds.* Arch Histol Cytol, 2006. **69**(3): p. 189-98.
81. Seta, Y., et al., *Mash1 is required for the differentiation of AADC-positive type III cells in mouse taste buds.* Dev Dyn, 2011. **240**(4): p. 775-84.
82. Matsuyama, K., et al., *Ascl1-expressing cell differentiation in initially developed taste buds and taste organoids.* Cell and Tissue Research, 2023. **392**(3): p. 631-641.
83. Hsu, C.-C., et al., *Mash1-expressing cells may be relevant to type III cells and a subset of PLCβ2-positive cell differentiation in adult mouse taste buds.* Cell and Tissue Research, 2021. **383**(2): p. 667-675.
84. Krishnamoorthy, N., et al., *Activation of c-Kit in dendritic cells regulates T helper cell differentiation and allergic asthma.* Nat Med, 2008. **14**(5): p. 565-73.
85. Li, M., et al., *c-kit is required for cardiomyocyte terminal differentiation.* Circulation research, 2008. **102**(6): p. 677-685.
86. Nasimi, M., et al., *SCF Improves In Vitro Differentiation of SSCs Through Transcriptionally Up-regulating PRTM1, STRA8, c-KIT, PIWIL2, and OCT4 Genes.* Reprod Sci, 2021. **28**(4): p. 963-972.
87. Liao, C.P., et al., *Identification of hair shaft progenitors that create a niche for hair pigmentation.* Genes Dev, 2017. **31**(8): p. 744-756.
88. Gerbe, F., et al., *Intestinal epithelial tuft cells initiate type 2 mucosal immunity to helminth parasites.* Nature, 2016. **529**(7585): p. 226-30.
89. Tomchik, S.M., et al., *Breadth of tuning and taste coding in mammalian taste buds.* Journal of Neuroscience, 2007. **27**(40): p. 10840-10848.
90. Travers, J.B., H.J. Grill, and R. Norgren, *The effects of glossopharyngeal and chorda tympani nerve cuts on the ingestion and rejection of sapid stimuli: An electromyographic analysis in the rat.* Behavioural Brain Research, 1987. **25**(3): p. 233-246.
91. St. John, S.J. and A.C. Spector, *Behavioral Discrimination between Quinine and KCl Is Dependent on Input from the Seventh Cranial Nerve: Implications for the Functional Roles of the Gustatory Nerves in Rats.* The Journal of Neuroscience, 1998. **18**(11): p. 4353.
92. Zaman, T., et al., *Kit Ligand and Kit receptor tyrosine kinase sustain synaptic inhibition of Purkinje cells.* eLife, 2024. **12**: p. RP89792.
93. Katafuchi, T., et al., *Impairment of spatial learning and hippocampal synaptic potentiation in c-kit mutant rats.* Learning & Memory, 2000. **7**(6): p. 383-392.

94. van Elst, J.M., et al., *Taste, smell and mouthfeel disturbances in patients with gastrointestinal stromal tumors treated with tyrosine-kinase inhibitors.* Support Care Cancer, 2022. **30**(3): p. 2307-2315.
95. Tizzano, M., et al., *Immunohistochemical Analysis of Human Vallate Taste Buds.* Chem Senses, 2015. **40**(9): p. 655-60.
96. Doty, R.L., *Chapter 15 - Psychophysical testing of smell and taste function*, in *Handbook of Clinical Neurology*, R.L. Doty, Editor. 2019, Elsevier. p. 229-246.
97. Chang, E., et al., *FDA Approval Summary: Tivozanib for Relapsed or Refractory Renal Cell Carcinoma.* Clin Cancer Res, 2022. **28**(3): p. 441-445.
98. Sánchez-Gastaldo, A., et al., *Systemic treatment of renal cell cancer: A comprehensive review.* Cancer Treatment Reviews, 2017. **60**: p. 77-89.
99. Lennartsson, J. and L. Rönnstrand, *Stem Cell Factor Receptor/c-Kit: From Basic Science to Clinical Implications.* Physiological Reviews, 2012. **92**(4): p. 1619-1649.
100. Klein, S., et al., *Interstitial cells of Cajal integrate excitatory and inhibitory neurotransmission with intestinal slow-wave activity.* Nature Communications, 2013. **4**(1): p. 1630.
101. Miyoshi, H. and T.S. Stappenbeck, *In vitro expansion and genetic modification of gastrointestinal stem cells in spheroid culture.* Nat Protoc, 2013. **8**(12): p. 2471-82.
102. Livak, K.J. and T.D. Schmittgen, *Analysis of relative gene expression data using real-time quantitative PCR and the 2(-Delta Delta C(T)) Method.* Methods, 2001. **25**(4): p. 402-8.

Acknowledgments
The authors thank the University of Colorado Organoid and Tissue Modeling Shared Resource (OTMSR) for providing WRN conditioned media and technical assistance for organoid experiments. The authors thank Dmitry Baturin and Lester Acosta of the University of Colorado Cancer Center Flow Cytometry Shared Resource for FACS, Trevor J. Isner and Amanda Stenzel for technical assistance with mouse and organoid experiments, and Thomas E. Finger, Katherine Fantauzzo, Heide Ford, Stephen Santoro, Santos Franco, Trevor J. Isner and Ian J. Purvis for helpful discussions and for critically reading the manuscript.

Funding:
National Institutes of Health T32GM141742 (CMP)
National Institutes of Health F31DC020634-01 (CMP)
National Institutes of Health R01DC018489 (LAB)
National Institutes of Health R01DC012383 (LAB)
National Institutes of Health R21CA236480 (LAB)
National Institutes of Health R01AI167923 (JVM)
National Institutes of Health P30CA046934 (CU OTMSR)
National Institutes of Health P30DK116073 (CU OTMSR)
National Institutes of Health P30CA046934 (CU Cancer Center)

Author contributions:
Project conceptualization: CMP, LAB, PJD, ETL
Organoid experiments: CMP, JKS
MATLAB coding and custom app creation: ES

Mouse handling: CMP, JKS, CEW
Tissue processing: CMP, JKS, ASH
Imaging and cell counting: CMP, ASH
Behavior: CMP, CEW, ASH
Generation of novel KIT10 allele: HIL, JVM
Writing: CMP, ES, LAB
Figure creation: CMP, LAB
Editing: all authors

Competing interests: Authors declare that they have no competing interests.

Data and materials availability: All data are available in the main text or the supplementary materials.